Ninth International Conference on Computational Fluid Dynamics (ICCFD9), Istanbul, Turkey, July 11-15, 2016

ICCFD9-xxxx

Temperature perturbation method to generate turbulent inflow conditions for LES/DNS simulations

Sophia Buckingham[1], Lilla Koloszar[1], Clara Garcia-Sanchez[1], Yann Bartosiewicz[2], Grégoire Winckelmans[2]

[1] von Karman Institute for Fluid Dynamics, Rhode-St-Genèse B-1640, Belgium

[2] Université catholique de Louvain, Institute of Mechanics, Materials and Civil Engineering, Louvain la Neuve 1348, Belgium

Corresponding author: sophia.buckingham@vki.ac.be

Abstract: An alternative approach to the classical velocity perturbations is applied to generate inflow turbulence for LES and DNS of wall bounded flows. The method consists in introducing random temperature perturbations that generate turbulence through local buoyancy effects. The cell perturbation method is implemented in the incompressible buoyant solver of OpenFOAM v2.3 and tested on a plane channel flow at $Re_\tau = 395$. The buoyancy force is locally increased within an active zone located at the entrance of the domain. The recovery length is minimized by optimizing the active zone specifications and the governing Richardson number. Reynolds stresses are compared to reference results. The method appears to be simple and efficient, while only first-order statistics are required as input.

Keywords: Large-Eddy Simulation, Turbulent inflow, Buoyancy, Temperature perturbations.

1 Introduction

The proper specification of turbulent inflow conditions for both Large Eddy Simulation (LES) and Direct Numerical Simulation (DNS) remains a considerable challenge. For developing flows, the most straightforward approach is to impose a laminar profile with small perturbations and to compute the transition to turbulence. However, simulating the transition process itself is very costly, and coupling this with a complex simulation of the downstream flow would be extremely expensive. The most common approach is to impose already a turbulent flow at the inlet. This too is a very difficult task since turbulent flows are coherent in both space and time. Thus, imposing inflow conditions that are physically correct and that satisfy the governing equations remains a considerable challenge. As a result, the flow needs to adjust until an equilibrium is reached. The key requirement for a turbulent inflow technique is to be as efficient as possible in order to minimize this recovery length and thus reduce the computational cost.

The existing techniques to generate inflow turbulence can be grouped into two main categories: precursor simulation methods and synthetic methods. Among the precursor simulation methods, two variants exist where the first consists in running an auxiliary calculation on a separate domain with periodic inlet-outlet boundary conditions, used for instance in [1] and [2]. The velocity in a section is stored at each time step; it is then fed at the inlet of the main domain that simulates the flow of interest. An important limitation, in addition to the need for an extensive database so that different flow regimes can be simulated, is that this approach is restricted to fully developed flows that rarely occur in reality. Moreover, the auxiliary simulation introduces "spurious" periodicity into the inflow as observed by Spille-Kohoff and Kaltenbach [3].
Cyclic or recycling methods are the second variant; these eliminate the necessity of generating a pre-computed

library by placing a cyclic plane in the inflow region of the actual computational domain. In the case of developing boundary layers, Lund et al. [4] proposed a procedure to rescale the velocity profile according to similarity laws before re-introducing it at the inlet. The computational effort of this second approach is reduced but, as precursor methods, the solution is affected by contamination due to periodicity. Attempts to remove these effects have been made by superimposing random perturbations, but results remain dependent on the characteristics of these random fluctuations.

Synthetic turbulence methods generate a pseudo-random coherent field of fluctuating velocities that tries to reproduce certain aspects of a turbulent flow. This requires the velocity field to be correlated both in time and space, with given first and second order moments, an assigned spectra, and the appropriate phase information between modes. While the moments and the spectra can be closely matched thanks to stochastic methods, the phase information strongly depends on the type of flow and location in the flow. It is therefore more difficult to specify but nevertheless crucial since the structure and shape of the turbulent eddies depend on it.
Different techniques exist to generate these random perturbations, such as proper orthogonal decomposition analysis (POD), Fourier decomposition, digital filter methods or Synthetic Eddy Method (SEM). POD techniques take as input instantaneous realizations of the flow acquired experimentally and extract basis functions that are optimal to represent the data and reconstruct turbulence. Perret et al. [5] used this method based on stereoscopic PIV measurements to provide inlet conditions for the LES of a mixing layer.
The Fourier or spectral methods use a decomposition of the signal into Fourier modes. Based on the work of Kraichnan [6], Smirnov et al. [7] proposed the random flow generation (RFG) technique that is implemented in Fluent as the Spectral Synthesizer [8]. It is able to generate an inhomogeneous and anisotropic turbulent flow, provided that an anisotropic velocity correlation tensor is specified. Modifications of the RFG method have been proposed by Keating et al. [9], adding a forcing term to amplify/damp velocity fluctuations in the wall-normal direction. Although the establishment length of the Reynolds stresses could be reduced by two along the channel down to about 10 half channel heights (δ), the turbulent kinetic energy needed a longer distance to reach its fully-developed value.
Another option is to use digital filtering. Xie and Castro [10] developed a digital filter that uses exponential functions in time and space for spatially developing boundary layers. LES of a plane channel provided satisfactory validation of the technique. In order to reduce the artificial pressure fluctuations introduced by the original turbulent inflow, Kim et al. [11] developed a divergence free version. This modification resulted in significantly reduced pressure fluctuations, however the recovery length for the skin friction coefficient for the channel simulation was increased to $16\,\delta$ instead of 10 with the original method of Xie and Castro [10].
Jarrin [12] proposed a synthetic eddy method (SEM) which creates velocity fluctuations by superposing eddies with random position and intensity. The author concluded that $15\,\delta$ were needed for the flow to recover equilibrium along a plane channel. Poletto et al. [13] derived a divergence free SEM (DFSEM) by modifying the shape function in the velocity computation. As a result, pressure fluctuations were almost eliminated while the recovery length along the channel was reduced by 33 % compared to the original method of Jarrin [12]. This latest reference also proposes a comprehensive review of several other methods to generate inflow turbulence, such as mixed methods that combine Fourier decomposition and digital filtering, forcing techniques or immersed boundary methods.

The important characteristics to consider while assessing turbulent inflow methods are the following:

1. What are the inlet parameters required by the method ?
2. Is the method divergence free, thus avoiding artificial pressure fluctuations ?
3. What is the skin friction recovery length needed to reach equilibrium ?

These questions are addressed in Table 1 for the main numerical methods and authors cited previously. The different inlet parameters are denoted as $< u >$ for the mean velocity, $< u_i u_j >$ for the Reynolds stresses, I_{ij} for the length and time scales, $< k >$ for the turbulent kinetic energy and N_{eddies} for the number of eddies.

To conclude, although the recovery length may be reduced to about $10\,\delta$ while satisfying divergence-free conditions, all of these turbulent inflow methods require *a priori* detailed information about the flow (i.e.,

Method	Author	Input parameters	Divergence free	Recovery length
Digital Filter	Xie & Castro [10]	$< u >$, $< u_i u_j >$, I_{ij}	no	$10\,\delta$
	Kim et al. [11]		yes	$16\,\delta$
Synthetic Eddy	Jarrin [12]	$< u >$, $< u_i u_j >$, I_{ij}, $< k >$, N_{eddies}	no	$15\,\delta$
	Poletto et al. [13]		yes	$10\,\delta$
Fourier (+forcing)	Smirnov [7]	$< u >$, $< u_i u_j >$	yes	$20\,\delta$
	Keating et al. [9]		yes	$10\,\delta$

Table 1: Overview of turbulent inflow methods

length scales, anisotropy or turbulence levels), that is unknown in a majority of cases. The purpose of the temperature perturbation method introduced in Section 2 is to propose a simple approach that only requires first order statistics, thus making it easily applicable to a variety of flows. Results of simulations on a plane channel flow are presented in Section 3 including a comparison with reference fully-developed turbulence obtained from a periodic inlet-outlet channel. Section 4 is dedicated to summary and concluding remarks.

2 Numerical methodology

2.1 The temperature perturbation method

The shortcomings of the existing turbulent inflow methods highlighted in Section 1 have motivated the development of alternative approaches that would be less complex and more flexible. In the frame of atmospheric boundary simulations, Mirocha et al. [14] introduced a new method based on the inclusion of random temperature perturbations. This technique relies on the principle that the seeded perturbations help to speed up turbulence generation by inducing local buoyancy effects. These vertical accelerations induce the creation of three-dimensional motions that eventually form turbulent structures. This method presents major advantages over the classical velocity perturbations. Instead of trying to impose realistic turbulence as boundary condition, turbulence is triggered through buoyancy, hence making the process naturally divergence-free. Moreover, it requires very limited information regarding the inlet flow specifications.
The temperature perturbations of Mirocha et al. [14] were sinusoidal in space and varied in size as a function of the model grid spacing. To limit their correlated aspect, the sign of the perturbations were reversed at specified frequencies. This approach was tested on a developing atmospheric boundary layer over a flat terrain. While encouraging results were obtained, exhibiting an accelerated development of turbulence compared to natural transition, further testing of the concept was required.

Thorough testing of the technique was carried out by Muñoz-Esparza [15] summarized in [16]. Four new approaches based on the temperature perturbation concept were proposed: spectral inertial subrange perturbations, spectral low wavelengths perturbations, point perturbations and cell perturbations. These were tested on a convective developing boundary layer and applied to the 24 first rows of cells located along the inlet boundary. The first two approaches perturbate the spectral distribution of temperature, while the last two impose spatial distributions; the spectral inertial subrange approach consists in perturbating essentially three modes that are located in the inertial subrange, in order to develop faster the energy-containing eddies. Similarly to a synthetic method, the spectral low wavelengths approach perturbates randomly the spectra obtained from a periodic simulation. The point and cell perturbation approaches consist in randomly perturbating the temperature in each cell or groups of cells respectively.
These four propositions were assessed by comparing their spectral behavior compared to a reference fully-developed periodic simulation. Results highlighted a spiky velocity spectrum in the case of the point perturbation method, suggesting that changing the random perturbations from one grid cell to another tends to excite the harmonics of the fundamental wavelength. The spectral inertial subrange method provided an enhanced energy content for the wavenumbers contained within the interval delimited by the three perturbated modes. These first two methods were clearly outperformed by the spectral low wavelengths and cell perturbation methods. Although larger levels appeared at intermediate wavelengths, their spectra were

found to be already close to the periodic inlet/outlet simulation after only $15x/z_{i0}$, z_{i0} being the temperature inversion height that limits the boundary layer height. Very similar energy distributions were obtained at $30x/z_{i0}$. The cell perturbation was preferred over the spectral low wavelengths as it requires less parallel communications, thus limiting the computational cost. It is therefore chosen in this study to investigate the generation of turbulent inflow conditions for LES simulations.

2.2 Application to wall bounded flows

2.2.1 Governing equations

Up to now, the temperature perturbation method has been applied to atmospheric boundary layer flows using the Weather Research and Forecasting (WRF) LES model [17]. The objective of this study is to apply the concept to incompressible wall bounded flows. The solver of OpenFOAM *buoyantBoussinesqFoam* is chosen to accommodate this technique as it models the buoyancy effects that will provoke the formation of turbulent structures by converting the seeded temperature gradients into velocity perturbations. The equations used by the solver are described hereafter. The constant-density filtered (LES) continuity equation is:

$$\frac{\partial \overline{u}_j}{\partial x_j} = 0 \tag{1}$$

The constant-density (except in the gravity term) filtered momentum equation is:

$$\frac{\partial \overline{u}_i}{\partial t} + \frac{\partial}{\partial x_j}(\overline{\overline{u}_i \overline{u}_j}) = -\frac{\partial}{\partial x_i}\left(\frac{\overline{p}}{\rho_0}\right) + \frac{\partial}{\partial x_j}(\overline{\tau}_{ij} + \overline{\sigma}_{ij}^{sgs}) + \frac{\overline{\rho}}{\rho_0} g_i \tag{2}$$

where g_i is the gravity vector, $\overline{\sigma}_{ij}^{sgs}$ is the subgrid-scale stress tensor and $\overline{\tau}_{ij}$ is the shear stress tensor due to molecular viscosity:

$$\overline{\tau}_{ij} = \nu_0 \left(\frac{\partial \overline{u}_i}{\partial x_j} + \frac{\partial \overline{u}_j}{\partial x_i}\right) \tag{3}$$

where ν_0 is the molecular kinematic viscosity. Note that, in OpenFOAM, the pressure is always normalized by the density for the incompressible solvers, such that $\overline{P} \triangleq \frac{\overline{p}}{\rho_0}$ is the kinematic pressure in $[m^2/s^2]$. Rearranging the gravity term, Eq. (2) can be rewritten as follows:

$$\frac{\partial \overline{u}_i}{\partial t} + \frac{\partial}{\partial x_j}(\overline{\overline{u}_i \overline{u}_j}) = -\frac{\partial \overline{P}}{\partial x_i} + \frac{\partial}{\partial x_j}\left[\nu_0 \left(\frac{\partial \overline{u}_i}{\partial x_j} + \frac{\partial \overline{u}_j}{\partial x_i}\right) + \overline{\sigma}_{ij}^{sgs}\right] + g_i \left(1 + \frac{(\overline{\rho} - \rho_0)}{\rho_0}\right) \tag{4}$$

The LES sub-grid scale stress tensor, $\overline{\sigma}_{ij}^{sgs}$, can be divided into a deviatoric part and an isotropic part, where $\overline{k}^{sgs} = -\frac{1}{2}\overline{\sigma}_{kk}^{sgs}$ is the LES sub-grid scale kinetic energy:

$$\overline{\sigma}_{ij}^{sgs} = \overline{\tau}_{ij}^{sgs} - \frac{2}{3}\,\overline{k}^{sgs}\delta_{ij} \tag{5}$$

The isotropic part can be placed in the first term on the right-hand side of Eq. (4), yielding a modified kinematic pressure $\tilde{P}$. The last term in parenthesis on the right-hand side of Eq. (4) can be expressed as follows:

$$1 + \frac{(\overline{\rho} - \rho_0)}{\rho_0} = 1 - \beta\left(\overline{T} - T_0\right) \tag{6}$$

where β is the thermal expansion coefficient in $[K^{-1}]$, $\overline{T}$ is the temperature in $[K]$ and T_0 is a reference temperature in $[K]$. As also usual in incompressible flows, the term $g_i \cdot 1$ can also be absorbed into the modified kinematic pressure: hence $\tilde{P} = \overline{P} + gy + \frac{2}{3}\,\overline{k}^{sgs}$. The deviatoric part of the subgrid-scale stress tensor is modeled as:

$$\overline{\tau}_{ij}^{sgs} = \nu_{sgs}\left(\frac{\partial \overline{u}_i}{\partial x_j} + \frac{\partial \overline{u}_j}{\partial x_i}\right) \tag{7}$$

where ν_{sgs} is the effective sub-grid scale kinematic viscosity. Substituting these different terms into Eq. (4) yields:

$$\frac{\partial \overline{u}_i}{\partial t} + \frac{\partial}{\partial x_j}(\overline{\overline{u}_i \overline{u}_j}) = -\frac{\partial \tilde{P}}{\partial x_i} + \frac{\partial}{\partial x_j}\left[\nu_{eff}\left(\frac{\partial \overline{u}_i}{\partial x_j} + \frac{\partial \overline{u}_j}{\partial x_i}\right)\right] - \beta\left(\overline{T} - T_0\right) g_i \tag{8}$$

where $\nu_{eff} = \nu_0 + \nu_{sgs}$ is the effective kinematic viscosity.

The filtered temperature equation can be written as:

$$\frac{\partial \overline{T}}{\partial t} + \frac{\partial}{\partial x_j}(\overline{\overline{T}\overline{u}_j}) = \frac{\partial}{\partial x_j}\left[\frac{k_0}{\rho_0 C_p}\frac{\partial \overline{T}}{\partial x_j}\right] + \frac{\partial}{\partial x_j}\left(\frac{k_{sgs}}{\rho_0 C_p}\frac{\partial \overline{T}}{\partial x_j}\right) \tag{9}$$

The right-hand side can be rearranged by recalling that $Pr = C_p\mu_0/k_0$ and by defining that $Pr_{sgs} = C_p\mu_{sgs}/k_{sgs}$, such that Eq. (9) becomes:

$$\frac{\partial \overline{T}}{\partial t} + \frac{\partial}{\partial x_j}(\overline{\overline{T}\overline{u}_j}) = \frac{\partial}{\partial x_j}\left[\left(\frac{\nu_0}{Pr} + \frac{\nu_{sgs}}{Pr_{sgs}}\right)\frac{\partial \overline{T}}{\partial x_j}\right] \tag{10}$$

The turbulent and molecular contributions to the heat transfer diffusivity are combined as:

$$\alpha_{eff} = \frac{\nu_{sgs}}{Pr_{sgs}} + \frac{\nu_0}{Pr} \tag{11}$$

with α denoting the thermal diffusivity. As is usual in LES, one assumes that Pr_{sgs} is constant.

2.2.2 Similarity parameters

The non-dimensional form of these governing equations can be obtained by scaling the variables as follows:

$$\overline{u}_i^* = \overline{u}_i/U_0;\ x_i^* = x_i/L_0;\ t^* = tU_0/L_0;\ \tilde{P}^* = \tilde{P}/U_0^2;\ (\Delta\overline{T})^* = (\overline{T} - T_0)/(\Delta T)_0;\ g_i^* = g_i/g_0 \tag{12}$$

with U_0, L_0, $(\Delta T)_0$ and g_0 that are reference quantities defining the problem.

This results in the dimensionless form of Eq. (8) for the momentum equation:

$$\frac{\partial \overline{u}_i^*}{\partial t^*} + \frac{\partial}{\partial x_j^*}(\overline{\overline{u}_i^*\overline{u}_j^*}) = -\frac{\partial \tilde{P}^*}{\partial x_i^*} + \frac{1}{Re}\frac{\partial}{\partial x_j^*}\left[\left(1 + \frac{\nu_{sgs}}{\nu_0}\right)\left(\frac{\partial \overline{u}_i^*}{\partial x_j^*} + \frac{\partial \overline{u}_j^*}{\partial x_i^*}\right)\right] - Ri\left(\Delta\overline{T}\right)^* g_i^* \tag{13}$$

where the Reynolds number, Re, gives the ratio between advective and viscous forces:

$$Re = \frac{U_0 L_0}{\nu_0} \tag{14}$$

and the Richardson number, Ri, gives the ratio between inertial and convective forces:

$$Ri = \frac{g_0\beta(\Delta T)_0 L_0}{U_0^2} \tag{15}$$

Similarly for the temperature equation, one obtains its dimensionless form as:

$$\frac{\partial \overline{T}^*}{\partial t^*} + \frac{\partial}{\partial x_j^*}\left(\overline{\overline{T}^*\overline{u}_j^*}\right) = \frac{1}{Pe}\frac{\partial}{\partial x_j^*}\left[\left(1 + \frac{\alpha_{sgs}}{\alpha_0}\right)\frac{\partial \overline{T}^*}{\partial x_j^*}\right] \tag{16}$$

where the Peclet number, Pe, is defined as:

$$Pe = Re\,Pr = \frac{U_0 L_0}{\alpha_0} \tag{17}$$

with the Prandtl number, Pr, giving the ratio between the momentum diffusivity and the thermal diffusivity, previously defined.

Referring to the momentum equation Eq. (13), one understands how the inclusion of temperature gradients can generate a buoyancy force that will induce the development of turbulent structures. The importance of these buoyancy effects are governed by the Richardson number, identified as a key parameter of the cell perturbation method.

2.3 Computational settings

The cell perturbation method proposed by Muñoz-Esparza [16] imposes random temperature perturbations along square bidimensional groups of cells. Through buoyancy effects, these have shown to induce the formation of three-dimensional turbulent structures. This research was extended (ref. [18]) with the objective of identifying and optimizing the governing parameters in order to reduce the recovery length.

2.3.1 Optimum perturbation range

In the case of compressible atmospheric flows, the contribution of the buoyancy force with respect to the mechanical forcing can be expressed by introducing a perturbation Eckert number:

$$Ec = \frac{U_0^2}{\rho_0 C_p \left(\Delta T\right)_{max}} \tag{18}$$

However, in the type of application treated here, the dimensional analysis of Section 2.2.2 does not make Ec intervene in the process since the dissipation function is considered as negligible for incompressible flows. Instead it is Ri that expresses the relative importance of the buoyancy effects. However, the work of Muñoz-Esparza [18] serves as reference to define the maximum perturbation amplitude, $(\Delta T)_{max}$, and deduce a recommended Richardson number. Different Eckert numbers were simulated by varying the perturbation range. An intermediate value of $Ec = 0.16$ insures an ideal balance between buoyancy and mechanical forcing, thus avoiding notable velocity distortion near the inflow which would result in a different quasi-equilibrium state. From this reference, an optimum Richardson number of $Ri = 0.3$ is obtained, representative of a mixed convection regime and taken as initial value in this study.

2.3.2 Optimum perturbation time scale

The perturbation time scale defines the frequency at which the perturbation values are changed. Thus, a dimensionless perturbation time scale (Γ) is proposed by Muñoz-Esparza [18], based on the perturbation time t_p:

$$\Gamma = \frac{t_p U_1}{d_c} \tag{19}$$

This parameter represents the time taken by the flow to be advected across a perturbation cell in the most adverse flow conditions. This is considering that the flow direction is along the diagonal of the perturbation cell, $d_c = \sqrt{2} n_c \Delta x$, with n_c the number of grid cells per perturbation cell side and Δx the cell size in the streamwise direction, for a velocity U_1 taken at the first vertical grid point.
The influence of this parameter on the results was investigated in [18], revealing that the performance of the method can be optimized by leaving sufficient time for the flow to assimilate the perturbations before imposing the next perturbations, such that $\Gamma = 1$. Indeed, for insufficient times ($\Gamma < 1$) the triggered instabilities were amplified, resulting in too much energy in the production range and longer distances to redistribute this energy content. If, on the contrary, $\Gamma >> 1$, the flow showed signs of loosing memory from one perturbation to the next, inducing alternating laminar and turbulent patches. Consequently, a value of $\Gamma = 1$ will be taken to calculate the perturbation frequency.

2.3.3 Spatial distribution of the perturbations

The temperature perturbations are distributed over a buffer region that starts from the inflow boundary. A uniform value is randomly attributed to tridimensional perturbation cells of $8\Delta x \times 8\Delta z \times 8\Delta z$ in the streamwise (x), wall-normal (y) and spanwise (z) directions respectively. The buffer region extends three

perturbation cells parallel to the inflow boundary, thus covering 24 grid cells in the streamwise direction. The perturbation cell size is chosen based on the study of Muñoz-Esparza [18] that recommends choosing a minimum size of $8\Delta x$ to avoid the energy from rapidly dissipating when applied to higher wavelengths. Higher sizes were also tested to study the impact of the perturbation cell size on the performance of the method. Although energy is placed into different scales, similar turbulent structures were observed in the flow, resulting in comparable transition lengths. Therefore, the perturbation cell size is not considered as critical and will be kept constant throughout this study.

A major difference compared to the previous application concerns the length scales involved. In atmospheric flows, even at a microscale level these may range from an order of magnitude of 10^{-1} to 10^{2} m, such that buoyancy effects are naturally present in these types of flows, with a typical Richardson number of $Ri = 0.3$. Wall bounded flows though involve smaller length scales ($< 10^{-1}$ m) and typically for air and limited gradients ($\Delta T < 1$ K), a plane channel flow simulation at $Re_\tau = 395$ is characterized by $Ri << 1$ and hence negligible buoyancy effects. Let us recall how the buoyancy force of Eq. (8) is defined in the current framework:

$$-\beta \left(\overline{T} - T_0\right) g_i \tag{20}$$

Since the purpose of the temperature method is to generate inflow turbulence without affecting the downstream flow in a significant way, some modifications of the temperature perturbation method are needed to fulfill both of these criteria. In particular, the buoyancy force needs to play an active role only close to the inflow region. To fulfill this requirement, the solution is to manipulate the thermal expansion ratio (β field) by artificially increasing its value within an active perturbation region at the inflow. This will enable the seeded perturbations to induce vertical accelerations that are sufficient to trigger the onset of three-dimensional motions and eventually accelerate the formation of turbulent structures. By setting β back to a realistic value outside of the active perturbation region, these effects will be rendered inactive downstream.

3 Validation on a plane channel flow

3.1 Numerical description

A plane channel flow is simulated with a domain size of $30\,\delta \times 2\,\delta \times 3.5\,\delta$, with δ the half channel height. The Reynolds number is set to $Re_\tau = 395$ based on δ and the friction velocity u_τ. A mesh of 1.68 Million cells is generated, with a number of grid points of $300 \times 80 \times 70$. The mesh is uniform in the streamwise and spanwise directions with resolutions of $\Delta x^+ = 39.5$ and $\Delta z^+ = 19.8$ respectively. A vertical stretching is applied in the wall-normal direction with an expansion ratio of 1.1 resulting in a first cell center at $y^+ = 0.9$. The Smagorinsky sub-grid scale model is applied with a constant coefficient $C_s = 0.065$ [19] and a van Driest wall damping [20]. A second order implicit scheme is used for time discretization and the time step is adjusted to insure that the CFL number reamins less than unity. A second order central discretization scheme is used for space discretization. The flow is solved by the buoyant incompressible solver *buoyantBoussinesqFoam* of OpenFOAM v2.3. The Poisson equation is solved so as to satisfy the continuity equation. It applies the PISO algorithm for pressure-velocity coupling, with two pressure corrector steps in this case. The solver is modified to include the temperature perturbation method, such that pseudo-random temperature perturbations are seeded every perturbation time step Δt_p, applying constant values to the predefined perturbation cells.
No-slip wall boundary conditions are applied to the top and bottom walls while periodic boundary conditions are applied in the spanwise direction. The mean velocity profile extracted from the periodic inlet/outlet channel simulation described in Section 3.2 is applied at the inlet. A zero velocity gradient is imposed at the outlet.
An aspect of the temperature perturbation method is to verify that, when introducing the perturbations, no net heat is added into the solution. This is checked by integrating the random values imposed over the perturbation cells.
Summarizing the guidelines formulated in Section 2.3 and followed in this study, the maximum amplitude of the temperature perturbations are set for $Ec = 0.16$ and the perturbation time is given by $\Gamma = 1$. The thermal expansion ratio (β) within the active perturbation region is modified from the fluid's value, β_{fluid},

to a so called active value, β_{active}, in order to retrieve $Ri = 0.3$. The influence of this zone is investigated in Section 3.3.

3.2 Reference periodic inlet/outlet channel

A LES simulation of a periodic inlet/outlet channel flow, referred to as case PBC, is first run for the selected $Re_\tau = 395$. The purpose of this preliminary simulation is to obtain a fully developed turbulent solution that provides a straightforward validation while testing the temperature perturbation method.
The mean velocity profile is the only input required by the temperature perturbation method; it is extracted from the periodic inlet/outlet simulation and imposed at the inlet. The corresponding Reynolds stresses will serve as reference while assessing the second moment statistics obtained with the inflow method at different streamwise locations along the channel.

The only modification compared to the numerical approach described previously consists in applying periodic boundary conditions between the inlet and the outlet. The flow is driven by a pressure gradient that is added to the streamwise momentum equation and adjusted to u_τ^2/δ in order to match the targeted Re_τ.
The mean velocity and Reynolds stress profiles obtained from case PBC are compared with reference DNS data [21] in Fig. 1. All profiles denoted by the superscript $^+$ are non-dimensionalized appropriately by the friction velocity u_τ and the kinematic viscosity ν.

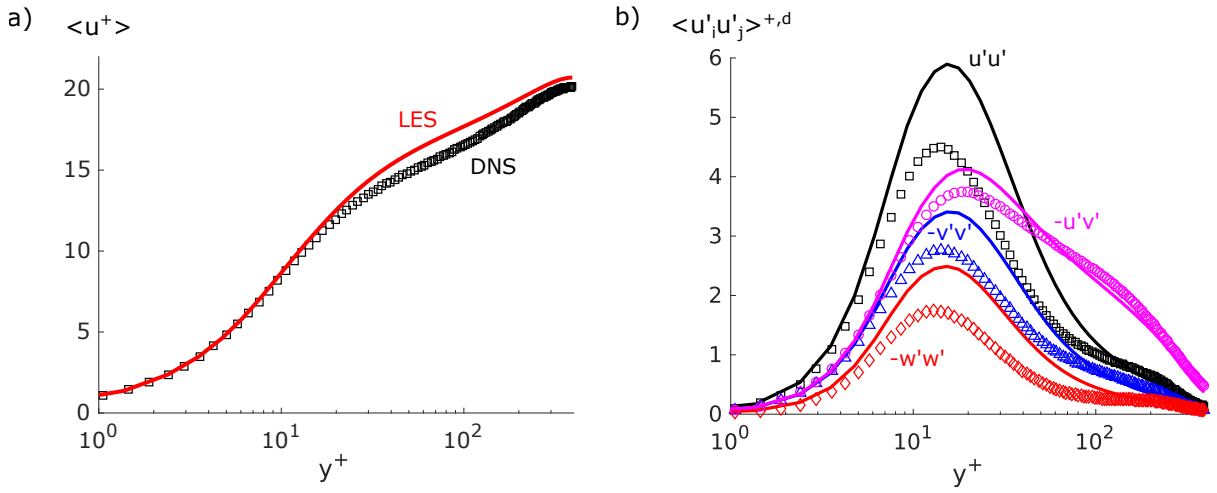

Figure 1: Profiles obtained from case PBC a) mean velocity b) Reynolds stresses. Here, deviatoric part for the diagonal elements: i.e. $< u'u' >^d = < u'u' > - \frac{1}{3}(< u'u' > + < v'v' > + < w'w' >)$. LES results (lines) and DNS data [21] (symbols)

As commonly observed in LES simulations with similar grid resolution [11], the mean velocity is over-predicted in the center of the channel, while $< u'u' >^+$ is over-predicted near the wall. On the contrary $< v'v' >^+$ is under-predicted in the near wall region [22]. However, the quality of the LES results remains satisfactory and despite these differences, the primary aim is to test the temperature perturbation method at a reasonable cost. Most importantly, case PBC remains the reference of the turbulent inflow channel.

3.3 Optimization of the turbulence development

3.3.1 Specifications of the perturbation zone

The focus of this section is to try and optimize the way the active perturbation zone introduced in Section 2.3.3 is defined. As a reminder, this region is characterized by an artificially high thermal expansion coefficient β, in order to generate a buoyancy force that is sufficient to perturbate the flow. To avoid having high temperature gradients that would still remain within the region of interest, the choice of keeping these

negligible was favored ($(\Delta T)_{max} < 1$ K) by increasing considerably the β field inside the active perturbation region.
The objective is to minimize the distance needed for the flow to adjust from the turbulent inflow section back to the equilibrium solution provided by the case PBC. This so-called recovery length is assessed based on the dimensionless wall shear stress, defined as $\overline{\tau}_w^+ = \overline{\tau}_w/(\rho u_\tau^2)$. In this case, a very strict error criteria of 0.5% is used to define the development length needed to retrieve the reference value of 1.

The first study concerns the inclusion of a buffer region at the transition between the fully active region, where β_{active} is applied from the inlet, to the rest of domain that is characterized by β_{fluid}. These are represented on the sketch of Fig. 2 hereafter:

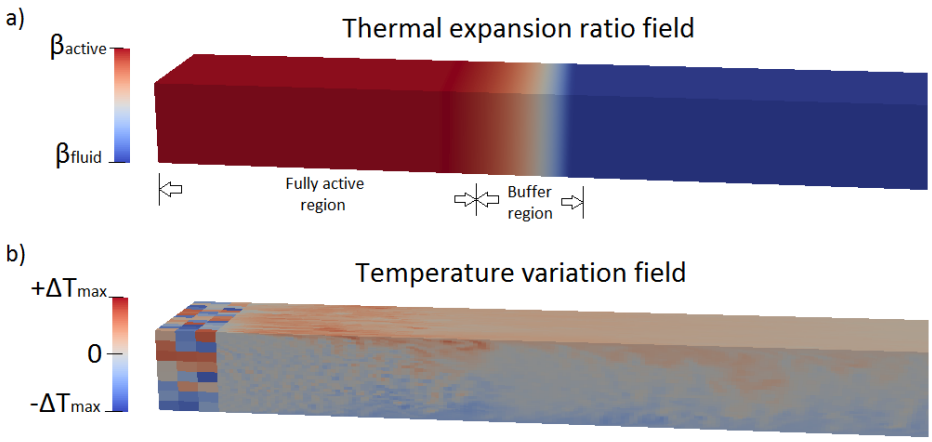

Figure 2: a) Contours of thermal expansion coefficient within the different regions b) Contours of temperature variation at a perturbation time step

Initially, the fully active region is $7\,\delta$ while the transition region extends until $10\,\delta$. Different smoothing functions are tested and the resulting development lengths are shown in Fig. 3. Among these, a linear damping (*linSmooth*), an exponential damping (*expSmooth*) and a double exponential damping (*dbExpSmooth*) are compared to the case without any smoothing (*noSmooth*).
The use of a buffer region appears to be beneficial since, without it, a strong peak appears at $7\,\delta$ where the sudden transition is located. Smoother functions at the top end or even at both ends do not prevent the buffer region from being felt by the wall shear stress. It is eventually the simplest smoothing corresponding to a linear function that is the most efficient, limiting the recovery length to $23.8\,\delta$.

Secondly, the length of the fully active region, L_{active}, is varied in an effort to further reduce the development distance. The initial value of $7\,\delta$ is compared to various lengths ranging from 3 to $10\,\delta$, keeping a linear transition of $3\,\delta$. The effect on the development of the wall shear stress is reported in Fig. 4 along with the associated recovery lengths top right. The results indicate that shortening the fully active zone increases the flow development. On the contrary, leaving more time for the flow to adjust enables to improve the development length by about 10%. Thanks to an active length of $10\,\delta$, the recovery length can be reduced down to $21.3\,\delta$.

Based on a reference total perturbation length of $13\,\delta$, the parametric study is finalized by looking into the influence of the buffer region length, L_{buffer}. Two additional configurations of $(L_{active} + L_{buffer})$ are tested, using values of $(5\,\delta + 8\,\delta)$ and $(7\,\delta + 6\,\delta)$. These are compared to the initial set-up of $(10\,\delta + 3\,\delta)$ in Fig. 5. A longer buffer length enables to shorten the recovery length, once again pointing out the necessity of having a smooth transition between the regions of the channel where the buoyancy effects are active and inactive. An optimum set-up is found for a fully active length of $5\,\delta$ and a buffer length of $8\,\delta$, for which the development length is equal to $19.4\,\delta$.

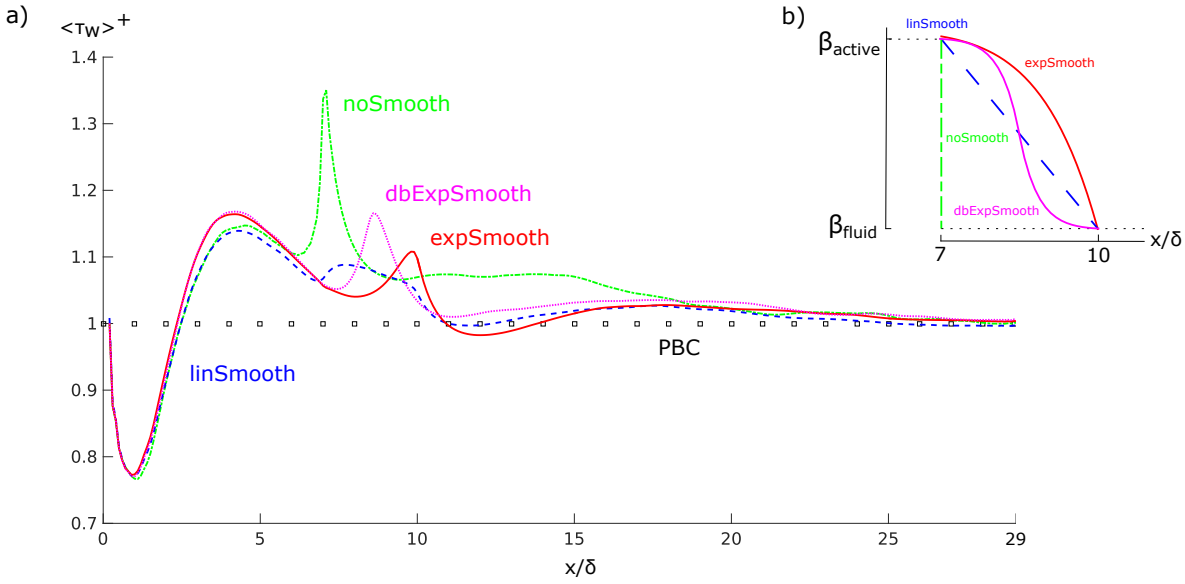

Figure 3: a) Effect of the transition region on the dimensionless wall shear stress b) Smoothing functions

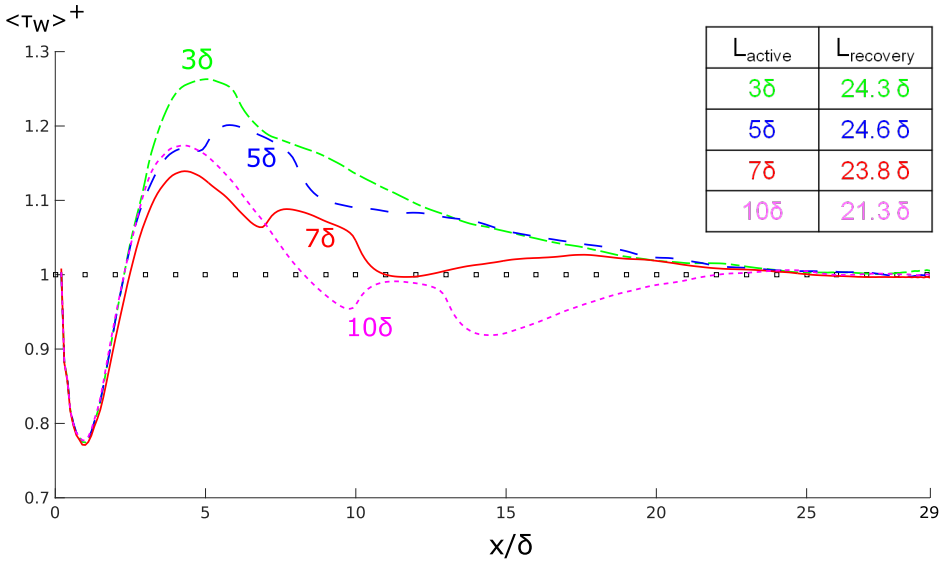

Figure 4: Effect of the fully active length on the dimensionless wall shear stress

3.3.2 Strength of the buoyancy effects

Identified in Section 2.2.2 as the key parameter governing the strength of the buoyancy effects, i.e. the influence of the Richardson number, is investigated in Fig. 6. Various values are tested around the initial value of 0.3 recommended by Muñoz-Esparza [18], keeping Ri within the range $[0.05 - 0.5]$.
The variations observed by the wall shear stress appear to strongly depend on the Richardson number. On one-hand, reduced buoyancy effects ($Ri = 0.1, 0.05$) slow down the transition process and, as a result, the flow takes longer to stabilized back to equilibrium. On the other-hand, an increase of Ri up to 0.5 amplifies the perturbations by introducing stronger stratification effects that will take slightly longer to dissipate along

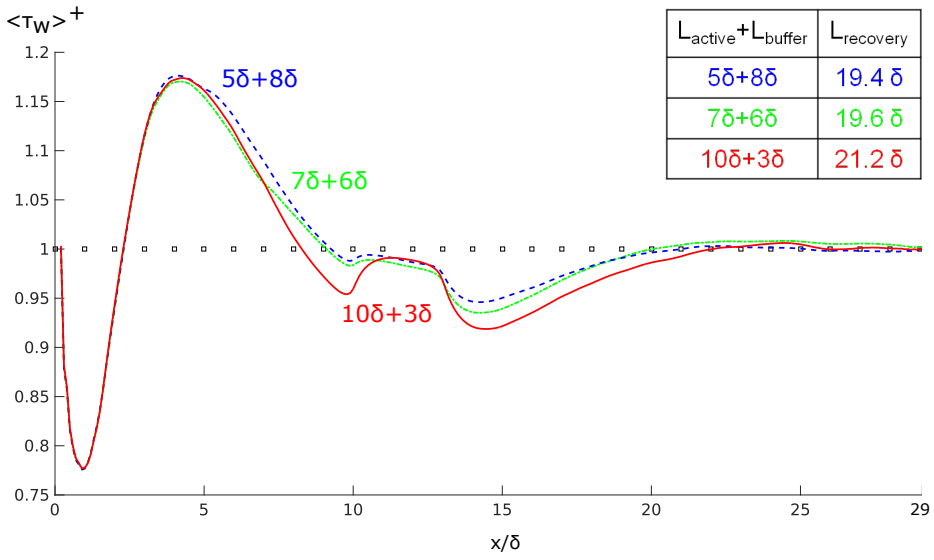

Figure 5: Effect of the total perturbation length on the dimensionless wall shear stress

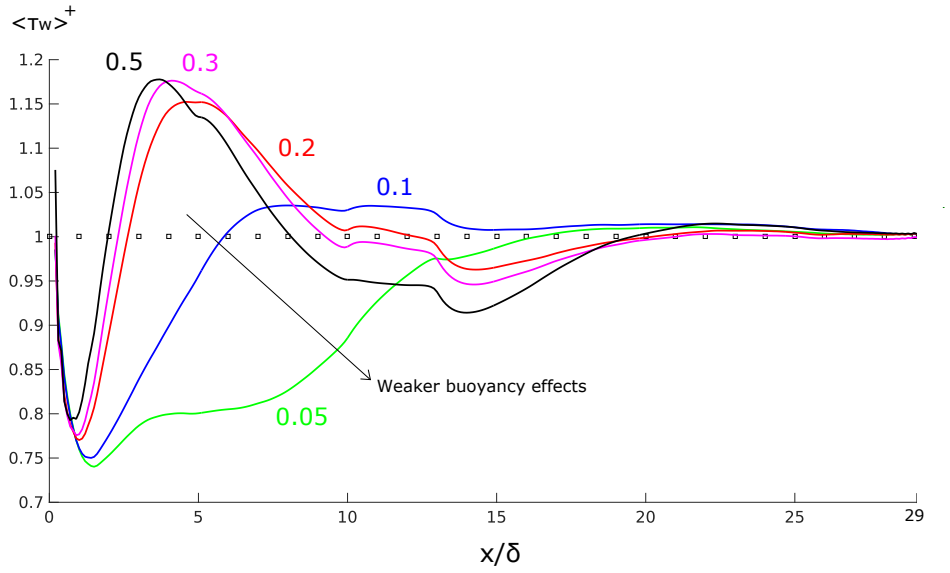

Figure 6: Effect of the total perturbation length on the dimensionless wall shear stress

the channel. To conclude, within the range of investigation, the variations in buoyancy effects have had a limited influence on the flow recovery. It is nevertheless recommended to keep the Richardson number within a range of $[0.2 - 0.3]$ in order to insure a recovery length of $20\,\delta$.

3.4 Turbulent flow solution

The turbulent flow that is generated by the temperature perturbation method is of primary interest. A first assessment of the flow development has been performed based on the recovery length of the wall shear stress. A thorough investigation is now proposed by analyzing the turbulent statistics. Fig. 7 provides the Reynolds shear stress along the channel, while the vertical profiles of velocity and Reynolds normal stresses

are provided in Fig. 8, at different streamwise locations. All dimensionless quantities are time and spanwise averaged.

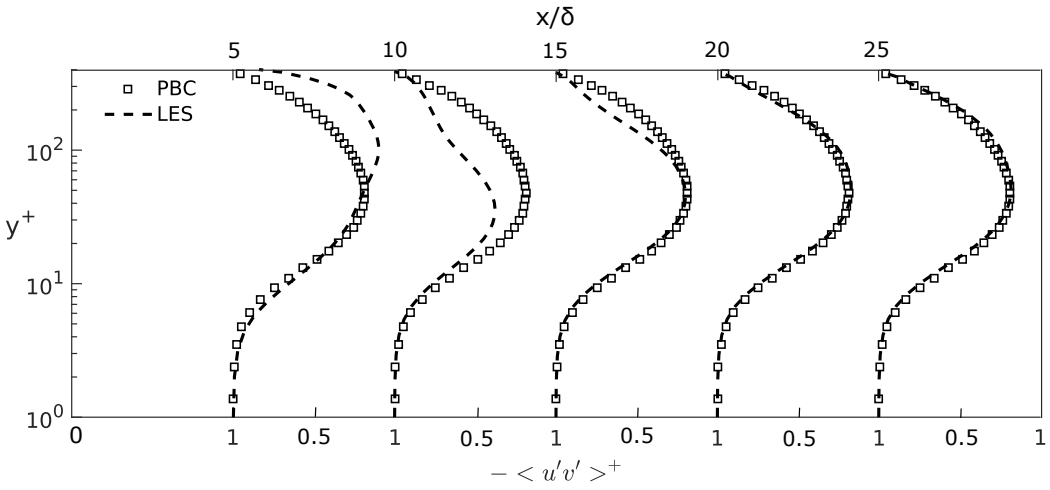

Figure 7: Vertical profiles of Reynolds shear stress -$< u'v' >^+$ along the channel

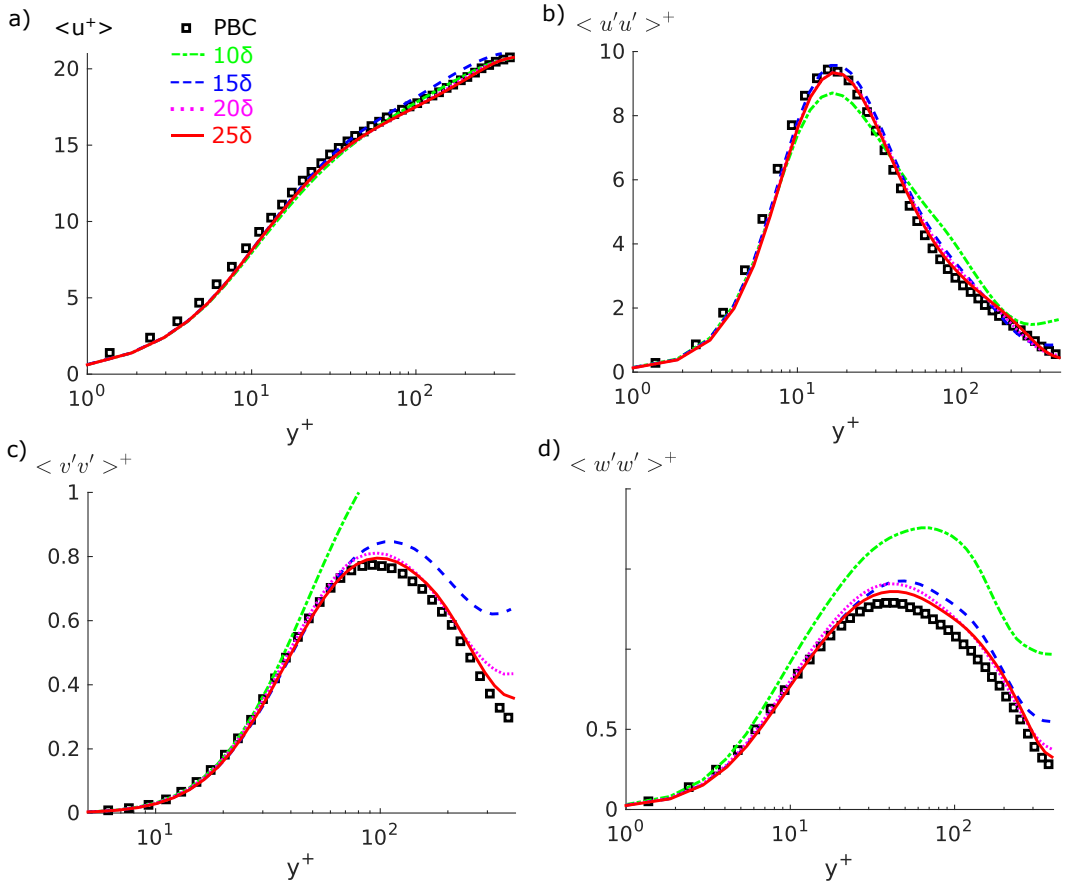

Figure 8: Turbulent statistics at different streamwise locations a) Velocity b)-d) Normal Reynolds stresses.

We recall that the first moment statistics are imposed at the inlet in the form of the mean velocity profile

obtained from case PBC. The turbulent inflow method has very little influence on this quantity and, already at $10\,\delta$ along the channel, the profile has converged back to the reference case PBC. Naturally, the second moment statistics take longer to reach equilibrium since the turbulent structures require a certain length to develop. Nevertheless, they show a good agreement with the reference at $15\,\delta$. The largest differences appear in the Reynolds stress normal to the wall $< v'v' >^+$, because of the vertical flow motions induced through buoyancy. These stratification effects are particularly visible towards the center of the channel and take longer to dissipate as the flow mixes downstream of the perturbation zone.

In accordance to the recovery length of $19.4\,\delta$ estimated previously, the flow development in terms of the recovery of Reynolds stresses is reached by $20\,\delta$. At this location, all profiles show satisfactory agreement with the case PBC representative of a fully developed turbulent state.

4 Conclusion and Future Work

An alternative technique that generates inflow turbulence for LES/DNS simulations applied to wall-bounded incompressible flows has been proposed. It consists in randomly perturbating the temperature in groups of cells placed at the inlet of the domain. The previously developed technique suited for atmospheric flows is modified by increasing the buoyancy forces within an active perturbation zone located in the upstream part of the domain. These effects then become sufficient to induce velocity perturbations and eventually the formation of coherent turbulent structures.

A parametric study has been carried out to improve the efficiency of the method and minimize the development distance in terms of the skin friction recovery and Reynolds stresses. The addition of a buffer region at the transition between the fully active zone, where the thermal expansion coefficient is artificially increased to retrieve sufficiently strong convective effects, and the rest of the fluid domain enables to insure a smoother transition. A linear smoothing in this area exhibits the best performance, and further improvements are attained by adjusting the lengths of the fully active region and buffer zone to $5\,\delta$ and $8\,\delta$ respectively. For this set-up, an optimum flow development distance of $20\,\delta$ is achieved.

To conclude, the temperature perturbation method appears to be a very promising approach to efficiently generate turbulence at the inflow. It presents major advantages over the classical velocity perturbation techniques by its simplicity and the fact that only first moment statistics (i.e. the velocity profile) are required as input. Future work will consist in proposing alternative ways of defining the perturbations in order to reduce stratification effects and further improve the efficiency of the method.

5 Aknowledgements

This work has been funded by the European MYRTE Horizon 2020 project (Contract number: 662186).

References

[1] N. Li, E. Balaras, and U. Piomelli. Inflow conditions for large-eddy simulations of mixing layers. *Phys. Fluids*, 12:935–938, 2000.

[2] U. Piomelli, E. Ballaras, and A. Pascarelli. Turbulent structures in accelerating boundary layers. *J. Turbul.*, 1:001, 2000.

[3] A. Spille-Kohoff and H.-J. Kaltenbach. Third AFOSR International Conference on DNS/LES Arlington, TX, 5-9 August 2001. In *Generation of turbulent inflow data with a prescribed shear-stress profile*, 2001. In DNS/LES Progress and Challenges, edited by C. Liu, L. Sakell, and T. Beutner.

[4] T. S. Lund. Generation of turbulent inflow data for spatially-developing boundary layer simulations. *J. of Computational Physics*, 140:233–258, 1998.

[5] L. Perret, J. Deville, R. Manceau, and J. Bonnet. Generation of turbulent inflow conditions for large eddy simulation from stereoscopic PIV measurements. *Int. J. Heat Fluid Flow*, 27:576–584, 2006.

[6] R. H. Kraichnan. Diffusion by a random velocity field. *Physics of Fluids*, 13:22–31, 1969.

[7] A. Smirnov, S. Shi, and I. Celik. Random flow generation technique for large eddy simulations and particle dynamics modeling. *J. Fluids Eng*, 71:123–359, 2001.

[8] ANSYS. *ANSYS FLUENT User's Guide*, 2011. Release 14.0.

[9] A. Keating, U. Piomelli, and E. Balaras. A priori and a posteriori tests of inflow conditions for large-eddy simulation. *Physics of Fluids*, 16(12):4696–4712, 2004.

[10] Z.-T. Xie and I. P. Castro. Efficient generation of inflow conditions for large eddy simulation of street-scale flows. *Flow Turbulence and Combustion*, 81(3):449–470, 2008.

[11] Y. Kim, I. P. Castro, and Z.-T. Xie. Divergence-free turbulence inflow conditions for large-eddy simulations with incompressible flow solvers. *Computers and Fluids*, 84:56–68, 2013.

[12] N. Jarrin. *Synthetic inflow boundary conditions for the numerical simulation of turbulence*. PhD Thesis, University of Manchester, Manchester, United-Kingdom, 2008.

[13] R. Poletto, T. Craft, and A. Revell. A new divergence free synthetic eddy method for the reproduction of inlet flow conditions for LES. *Flow Turbulence and Combustion*, 91:519–539, 2013.

[14] J. Mirocha, B. Kosovic, and G. Kirkil. Resolved tubulence characteristics in large-eddy simulations nested within mesoscale simulations using the Weather Research and Forecasting model. *Mon. Weather Rev.*, 142:806–831, 2014.

[15] D. Muñoz-Esparza. *Multiscale modelling of atmospheric flows: towards improving the representation of boundary layer effects*. PhD Thesis, Université Libre de Bruxelles - von Karman Institute for Fluid Dynamics, Brussels, Belgium, 2013.

[16] D. Muñoz-Esparza, B. Kosovic, J. Mirocha, and J. van Beeck. Bridging the transition from mesoscale to microscale turbulence in numerical weather prediction models. *Boundary Layer Meteorol.*, 153:409–440, 2014.

[17] W. Skamarock, J. Klemp, J. Dudhia, D. Gill, D. Barker, M. Duda, X. Huang, W. Wang, and J. Powers. A description of the advanced research WRF version 3. NCAR Tech. Note NCAR/TN-475+STR, 2008.

[18] D. Muñoz-Esparza, B. Kosovic, J. van Beeck, and J. Mirocha. A stochastic perturbation method to generate inflow turbulence in large-eddy simulation models: Application to neutrally stratified atmospheric boundary layers. *Physics of Fluids*, 27(035102), 2015.

[19] P. Moin and J. Kim. Numerical investigation of turbulent channel flow. *J. Fluid Mech.*, 118:341–377, 1982.

[20] E. R. van Driest. On turbulent flow near a wall. *AIAA*, 23:1007–1011, 1956.

[21] R. D. Moser, J. Kim, and N. N. Mansour. Direct numerical simulation of turbulent channel flow up to $Re_\tau = 590$. *Phys. Fluids*, 11:943–945, 1999.

[22] G. S. Winckelmans, H. Jeanmart, and D. Carati. On the comparison of turbulence intensities from large-eddy simulation with those from experiment or direct numerical simulation. *Brief Comm. in Phys. Fluids*, 14(5):1809–1811, 2002.